

Journal of Materials Chemistry B

Accepted Manuscript



This article can be cited before page numbers have been issued, to do this please use: A. Galstyan and U. Dobrindt, *J. Mater. Chem. B*, 2018, DOI: 10.1039/C8TB01357H.



This is an Accepted Manuscript, which has been through the Royal Society of Chemistry peer review process and has been accepted for publication.

Accepted Manuscripts are published online shortly after acceptance, before technical editing, formatting and proof reading. Using this free service, authors can make their results available to the community, in citable form, before we publish the edited article. We will replace this Accepted Manuscript with the edited and formatted Advance Article as soon as it is available.

You can find more information about Accepted Manuscripts in the [author guidelines](#).

Please note that technical editing may introduce minor changes to the text and/or graphics, which may alter content. The journal's standard [Terms & Conditions](#) and the ethical guidelines, outlined in our [author and reviewer resource centre](#), still apply. In no event shall the Royal Society of Chemistry be held responsible for any errors or omissions in this Accepted Manuscript or any consequences arising from the use of any information it contains.



Journal Name

ARTICLE

Breaching the wall: morphological control of efficacy of phthalocyanine-based photoantimicrobials

Anzhela Galstyan^{*a} and Ulrich Döbrindt^bReceived 00th January 20xx,
Accepted 00th January 20xx

DOI: 10.1039/x0xx00000x

www.rsc.org/

Efficient treatment of infections using antimicrobial photodynamic therapy (aPDT) anticipates that uptake of photosensitizer (PS) by bacterial cells is very fast and effective. In this work design, synthesis, characterization, and photodynamic activity of amphiphilic, water-soluble zinc(II) phthalocyanines (Zn(II)Pc) bearing none, three or six thiophenyl moieties are described. We show that PSs that contain no or flexible substituents on non-peripheral positions can photoinactivate microbes at very low loading concentrations and low light doses. Contrary, a PS derivative that contains non-flexible substituents is rendered less effective, despite an increased generation of cytotoxic singlet oxygen, higher lipophilicity and lower tendency to aggregate. Our unexpected finding emphasizes the role of the morphology of PS in bacterial cell-molecule interaction and suggests another relevant and hitherto disregarded characteristic to improve PS design.

Introduction

Antimicrobial photodynamic therapy (aPDT) is a gradually expanding approach that enables fast and very effective treatment of bacterial infections.^{1,2} Efficient and reliable PS for aPDT have emerged over the last few decades to meet this demand.³⁻⁵ A good PS is expected to fulfill many essential characteristics, such as ability to absorb light energy in the spectral range of visible and near infrared light (600 – 800 nm) characterized by a high penetration depth into the tissues and transfer it to substrate (e.g. oxygen), high extinction coefficients, tunable photophysical properties, low dark toxicity, selectivity towards bacterial cells, etc. Localization and distribution of PSs are significant in determining antimicrobial activity and it is assumed that these depend on two PS features: affinity for the cellular components and amphiphilic character.⁶ An important challenge remains beyond the simple correlation of PS lipophilicity and photodynamic efficacy, namely establishing the role of the molecule's shape and flexibility of the substituents on photodynamic efficacy. Numerous studies have shown that photoinactivation of Gram-negative bacteria is particularly challenging.⁷ Although bacterial cells are far less advanced than mammalian cells, the composition of the cell wall of Gram-negative bacteria is very

complex: it contains two membranes, with a thin peptidoglycan layer spanning the periplasm and lipopolysaccharide (LPS) chains embedded on the surface layer of the outer membrane (Figure 1b). In order to be sensitive to the photosensitized destruction, PS should efficiently bind to or pass through one or more of these barriers.⁸ Despite the evidence that internalization of PS is not required per se, literature review indicates that PS, which can plunge into the oxygen-rich lipid bilayer, is able to inactivate bacteria at very low concentrations and low light doses.^{9,10} While Gram-negative bacteria frequently produce outer membrane vesicles, endocytosis-like membrane-trafficking is hindered by its asymmetric lipid architecture and the peptidoglycan layer. Protein transport machineries such as porin channels can mediate PS uptake,¹¹ however, they have threshold sizes of transportable molecules¹² (generally < 600 Da). Though, positive charges of PS promote interactions with anionic groups at the external surfaces of the microbial target it was considered that further translocation via self-promoted uptake pathway is determined by the hydrophobicity of the PS. In the present study, we clearly show for the first time, that the morphology of the chromophore plays an important role in PS translocation across bacterial cell membranes and consequently has a big impact on its photodynamic efficacy. The amphiphilic nature of PSs is one of the most desired features and is frequently used to promote hydrophobic interactions with the outer membrane of bacteria.¹³ Most commonly the chromophore unit carries a positive charge whereas hydrophobic side groups are introduced to direct the PS to the interior of the bacterial cell.¹⁴⁻¹⁶ However, an enormous increase of activity was observed when charged groups were a part of an auxochromic side chain.^{9,17} Most likely direct and efficient interaction of the chromophore with

^aCenter for Soft Nanoscience, Westfälische Wilhelms-Universität Münster, Busso-Peus-Straße 10, D-48149 Münster, Germany.
E-mail: anzhela.galstyan@wwu.de,

^bInstitute of Hygiene, Westfälische Wilhelms-Universität Münster, Mendelstraße 7, D-48149 Münster, Germany.

† Footnotes relating to the title and/or authors should appear here.

Electronic Supplementary Information (ESI) available: [details of photophysical characterization, DFT calculations and photobiological studies]. See DOI: 10.1039/x0xx00000x

ARTICLE

Journal Name

the PDT-sensitive membrane is contributing to the increased antibacterial effect.

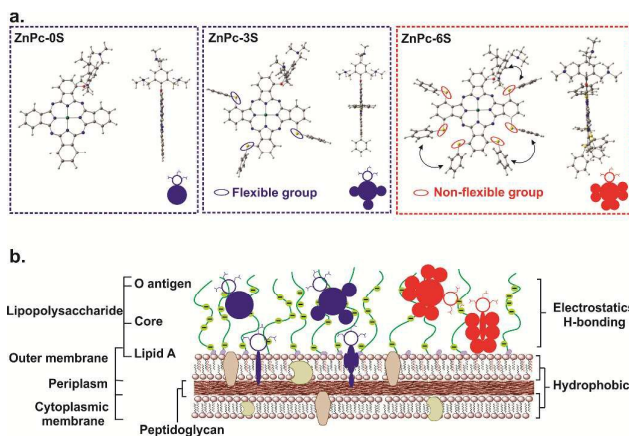


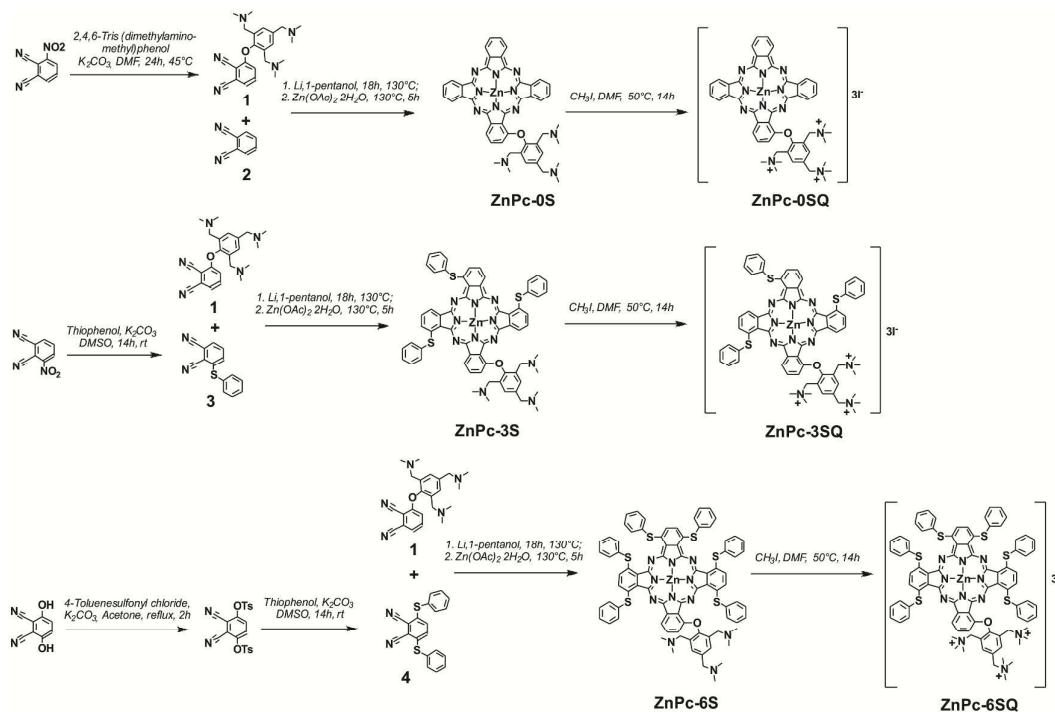
Fig. 1. (a) Optimized structures of ZnPc-0S, ZnPc-3S, ZnPc-6S at the B3LYP/6-31G(d,p) level of theory, (b) schematic representation of cell wall composition of Gram-negative bacteria and its interaction with ZnPcs.

Phthalocyanines (Pc) are one of the most studied PSs with an intense $\pi \rightarrow \pi^*$ absorption in the visible spectrum.¹⁸ By changing number, position, and nature of the substituents it is possible to shift the Q band in Uv-vis spectra to the longer wavelength that corresponds to the tissue transparency window and is highly desirable for PDT applications. Kobayashi *et al.* demonstrated that the incorporation of group 16 (S, Se and Te) elements at the non-peripheral positions of the Pc

core results in a large red shift of the Q-band.¹⁹ Additionally, such a ring modification also contributes to the efficient photosensitized generation of singlet oxygen due to the increase in intersystem crossing efficacy and fast formation of lowest triplet state due to the “heavy atom effect”.²⁰ In this paper photophysical, theoretical and biological studies are combined, highlighting importance of different characteristics for design of new and more effective PSs.

Results and discussion

A series of amphiphilic low-symmetry Zn(II)Pcs with A₃B type construction that contain no (ZnPc-0S), three (ZnPc-3S) or six (ZnPc-6S) thioaryl substituents on the unit A and one 2,4,6-tris(dimethyl aminomethyl)phenyl substituent on the unit B were prepared. The starting 3-[2,4,6-tris(N,N-dimethylaminomethyl)phenoxy] phthalonitrile,²¹ 3-phenylthio phthalonitrile,²² 3,6-bis(tosyloxy) phthalonitrile and 3,6-bis(phenylthio) phthalonitrile^{19a} were synthesized and purified by known procedures. The classical synthetic approach was used towards unsymmetrically substituted phthalocyanines, which implies the cross-condensation of unit A and unit B in a 4 : 1 molar ratio following so-called lithium method. Zn(II)Pcs were obtained through metal insertion reaction of the free base phthalocyanine with zinc acetate salt and the complexes ZnPc-0S, ZnPc-3S and ZnPc-6S were isolated by silica gel column chromatography. To achieve solubility in a wide pH range dimethylamino groups were further quaternized with methyl iodide leading to the formation of ZnPc-0SQ, ZnPc-3SQ, and ZnPc-6SQ, correspondingly (Scheme 1).



Scheme 1. Synthetic pathway towards Zn(II)Pcs used in this study.

Journal Name

ARTICLE

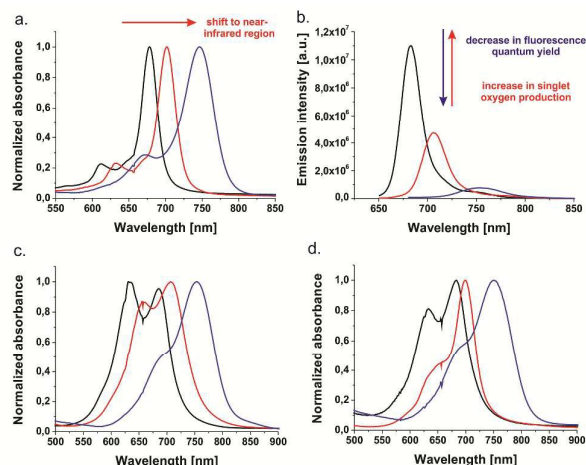


Fig. 2. a. Optical absorbance of ZnPc-0S (black), ZnPc-3S (red) and ZnPc-6S (blue) in DMF normalized to the same absorptivity for the lowest energy Q-band; b. fluorescence emission spectra of ZnPc-0S (black), ZnPc-3S (red) and ZnPc-6S (blue) in DMF (normalized for absorbance values ~ 0.08); c. normalized absorption spectra of ZnPc-0S (black), ZnPc-3S (red) and ZnPc-6S (blue) and d. ZnPc-0SQ (black), ZnPc-3SQ (red) and ZnPc-6SQ (blue) at the concentration 1×10^{-5} M in water.

As expected, introduction of thiophenyl substituents into α -positions of the Pc macrocycle had a substantial influence on the aggregating behaviour and photophysical characteristics of Zn(II)Pcs. Whereas these compounds were present in a monomeric form in DMF, as indicated by a sharp absorption Q-band, they were substantially aggregated in aqueous media (Fig. 2). A broad shoulder at lower wavelengths, which is typical for H-type aggregate formation, was more pronounced for ZnPc-0S, ZnPc-0SQ and ZnPc-3S. In contrast, the intensity ratio of the first two vibronic peaks in the absorption spectra of ZnPc-3SQ, ZnPc-6S and ZnPc-6SQ increased (Fig. 2c and 2d). Thus the quaternization of the dimethyl amino groups and/or

introduction of sterically demanding substituents can substantially suppress chromophore stacking.²³

To gain insights into the stability of PSs, we compared photobleaching (photodegradation) of ZnPc-0S, ZnPc-3S and ZnPc-6S upon continuous illumination with $\lambda > 610$ nm light with 30 mW/cm² flow rate and recorded the decrease in the Q-band of the UV-vis spectra. Photodegradation was found to be more pronounced in DMF for all Zn(II)Pc derivatives since DMF is known to be less efficient in stabilizing the ring against oxidative attack. Notably, comparing photobleaching of PSs in H₂O, the largest photobleaching was observed for ZnPc-0S (Fig. S5, ESI†).

A varying number of the thiophenyl substituents (0-3-6) impacted the absorption and emission maxima of Zn(II)Pcs. Compared to Q band absorption of ZnPc-0S at 678 nm in DMF, the introduction of the electron-donating sulfur atoms in α -positions of the macrocycle induced a red-shift of the Q band absorption; ZnPc-3S at 702 nm and ZnPc-6S at 754 nm in DMF. The quaternized derivatives exhibited their Q band absorptions at very similar positions to that of uncharged derivatives (Table 1). A similar trend in the red-shift was observed in the fluorescence spectra of Zn(II)Pcs (Fig. 2b). The highest fluorescence quantum yield (Φ_F) was observed for ZnPc-0S. Dyes containing sulfur bridges showed an obvious decrease in Φ_F , while at the same time singlet oxygen quantum yields (Φ_Δ) were increased, which points to a very rapid intersystem crossing from the singlet to the triplet excited state. Quaternization of dimethylamino groups affected the photophysical properties such as Φ_F and Φ_Δ . For ZnPc-0SQ and ZnPc-3SQ the values of Φ_F were decreased, while the increase of values of Φ_Δ was observed. For ZnPc-6SQ differences to unquaternized derivative were not significant. In respect to the number of thiophenyl substituents, both values followed the rule of the heavy atom effect as in case of an-quaternized derivatives (Table 1).

Table 1. Photophysical data for zinc(II)phthalocyanines used in this study

PS	$\lambda_{\text{abs}}/\text{nm}$ (log10 ϵ)	$\lambda_{\text{em}}/\text{nm}$ ^[a]	$\Phi_F \pm 0.02$ ^[b]	$\Phi_\Delta \pm 0.03$	LogPo/w
ZnPc-0S	678 (5.01), 611 (4.36), 336 (4.58)	683	0.25	0.43 ^[c]	0.05
ZnPc-0SQ	675 (5.08), 609 (4.48), 342 (4.67)	682	0.20	0.66 ^[c] /0.61 ^[d]	-0.53
ZnPc-3S	702 (5.02), 631 (4.32), 332 (4.39)	708	0.09	0.61 ^[c]	0.14
ZnPc-3SQ	701 (5.00), 630 (4.33), 333 (4.42)	705	0.06	0.72 ^[c] /0.76 ^[d]	-0.44
ZnPc-6S	754 (4.90), 678 (4.39), 346 (4.52)	758	0.02	0.93 ^[c]	0.23
ZnPc-6SQ	753 (4.93), 677 (4.65), 349 (4.80)	758	0.02	0.89 ^[c] /0.81 ^[d]	-0.19

^[a]Excited at 610 nm (ZnPc-0S), 630 nm (ZnPc-3S) and 660 nm (ZnPc-6S). ^[b]Quantum yields were calculated by the steady state comparative method using zinc(II)phthalocyanine as a reference ($\Phi_F = 0.28$ in DMF). ^[c]Quantum yields were measured in DMF using the relative method and zinc(II)phthalocyanine ($\Phi_F = 0.56$) as a reference. ^[d]Quantum yields were measured in H₂O using the relative method and methylene blue ($\Phi_F = 0.52$) as a reference.

Journal Name

ARTICLE

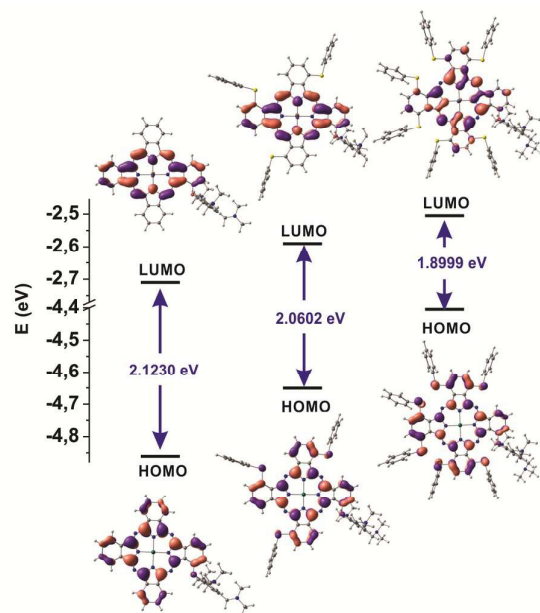


Fig. 3. DFT-predicted energy diagram for the frontier MOs in ZnPc-0S, ZnPc-3S and ZnPc-6S (B3LYP/6-31G(d,p)). The surfaces of selected orbitals are also depicted.

In order to further investigate the photophysical nature of these novel PSs and rationalize experimental observations, density functional theory (DFT) and time dependent density functional theory (TD-DFT) calculations at B3LYP/6-31G(d,p) level were employed. Morphology, frontier orbitals and excited states of PSs were studied. Optimized molecular geometries are shown in Fig 1 and cartesian coordinates are given in ESI†. The absence of any imaginary frequencies confirms that our optimized structures are local minima. Though in both ZnPc-3S and ZnPc-6S dihedral angles of phenyl substituents are close to 90°, more flexible nature of phenyl moieties in ZnPc-3S allows for a more flat geometry of the PS molecule. In this case, PS can adopt planar configuration upon interaction with the biological target (vide infra). Contrary, in the case of ZnPc-6S rotation of the phenyl moiety is restricted. Moreover, great steric hindrance leads to a distorted conformation of the Pc ring. Similar distortions were also observed in symmetrically 1,4,8,11,15,18,22,25-octa substituted Pcs contacting bulky substituents.²⁴ In agreement with the experiment, TD-DFT calculations correctly predicted a stepwise reduction of the highest occupied molecular orbital (HOMO) – lowest unoccupied molecular orbital (LUMO) energy gap in the asymmetric system in the order of ZnPc-0S (2.12 eV) > ZnPc-3S (2.06 eV) > ZnPc-6S (1.90 eV) (Fig. 3). Table 2 lists theoretical electronic parameters of all PSs. ZnPc-3S and ZnPc-6S exhibited the destabilization of the HOMO and LUMO levels

in comparison with ZnPc-0S due to the electron donating nature of the sulfur. Uv-vis spectra generated from the B3LYP/6-31G(d,p) calculated data correlated well with the observed red shifts of the Q-bands in the experimentally measured Uv-vis spectra (see ESI†).

Table 2. Energy differences predicted in the TD-DFT calculations ($\Delta(E_L - E_H)$), calculated excited wavelength (λ), oscillator strengths (f) and composition.

PS	$\Delta(E_L - E_H)$ (eV)	λ (nm)	f	Composition
ZnPc-0S	2.1230	605.35 602.42	0.5276 0.3835	H→L (69 %) H→L+1 (69 %)
ZnPc-3S	2.0602	643.22 639.88	0.5348 0.5372	H→L (69 %) H→L+1 (69 %)
ZnPc-6S	1.8999	720.33 717.75	0.4569 0.5945	H→L (43 %) H→L+1 (55 %) H→L (55 %)

Antimicrobial photodynamic efficacies of novel PSs against *E. coli* UTI89 and *E. coli* 536 were assessed after incubation with 1 and 10 μ M solutions of corresponding PS for 15 min at 37°C. Light activation of ZnPc-0SQ and ZnPc-3SQ resulted in a rapid reduction of viable bacterial numbers of both *E. coli* strains with a light dose as low as 3 J cm⁻². When ZnPc-6SQ was as PS under the same conditions reduction of colony forming units (CFU) was lower, even at the highest concentration of 10 μ M (Fig. 4). These results were not anticipated considering known criteria of “chemical input – biological output”. Given that the interaction between the target organism and the PS is essential to successfully kill the bacterial cell, the differences in activity among the derivatives may be attributed to the different binding sites of Zn(II)Pcs.

As a possible mechanism of action against Gram-negative bacteria, we propose that PSs non-covalently associates with outer membrane components such as lipopolysaccharides and capsular polysaccharides, and crosses relatively flexible and dynamic part of the outer membrane. Later, most likely, morphological reorganization occurs in contact with the rigid outer membrane. The chromophore unit of ZnPc-0S is planar and ZnPc-3S can adopt a planar conformation, considering that due to the steric effect the statistical formation of the C_{4h} symmetry form is preferred. This enables membrane accumulation of ZnPc-0S and ZnPc-3S, leading to a very rapid killing kinetics upon irradiation. Geometrical parameters obtained for ZnPc-6S after total optimization by B3LYP/6-

31G(d,p) (Figure 1a) indicate that molecular rotations of phenyl substituents on non-peripheral positions of the macrocycle were restricted and thus intramolecular planarization of ZnPc-6S is not possible. For this reason, ZnPc-6S cannot efficiently accumulate in the oxygen-rich outer membrane of *E. coli* cells, being unable to effectively focus its photosensitizing potential.

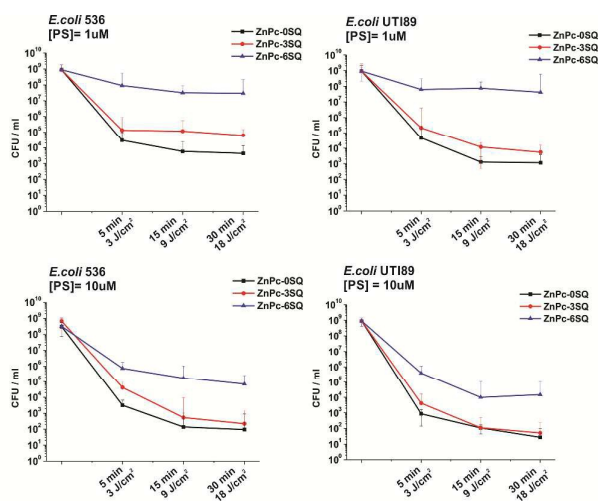


Fig. 4. Photoinactivation of *E. coli* 536 and UT189 treated with PSs and irradiated with visible light (> 610 nm, 10 mW/cm 2).

Unlike membrane-active antimicrobials, such as peptides and their synthetic mimics, general or local destabilization of the target membrane without illumination is not desired for PSs and can lead to unwanted dark toxicity. So the question arises, how important is internalization of PSs into the bacterial cell? Ultimately, to answer this question structure activity parameters of many different PSs need to be compared. Generally highly symmetric PSs such as tetracationic Zn(II)Pcs containing *N*-methylpyridyloxy²⁵ and trimethylaminophenoxy moieties (known as RLP068/Cl)²⁶ show satisfying outcome (*E. coli*, 4.5 log, 10 μ M, 54 J/cm 2 and *P. aeruginosa*, 5–6 log, 26.4 μ g/ml, 30 J/cm 2 , correspondingly). However, oligolysine-conjugated Zn(II)Pc that has been tested against *E. coli* was found to have a much higher activity out of a range of different cationic ZnPcs (4 log, 0.8 μ M, 48 J/cm 2). In this case the Pc ring was substituted only in one di- λ position of the Pc core and the chromophoric Pc ring could achieve effective binding to the cell membrane via hydrophobic interactions.²⁷ Similarly, monosubstituted ZnPc, a structural analogue of ZnPc-0S, also exhibited a high potency against a range of Gram-negative *E. coli* upon illumination with red light (0.3 – 1.3 μ M, 4 log, 54 J/cm 2).¹⁸ Recently computer simulations of the interaction of chlorine-substituted Zn(II)Pc with bacterial membrane shows that Zn(II)Pc molecules became adsorbed within the first 5 μ s. Subsequently, one of the Pcs was translocating towards the membrane center over the following 2.5 μ s, changing its orientation from predominantly parallel to the membrane surface to perpendicular.²⁸ The authors also show that

translocation of Zn(II)Pc into the outer bacterial membrane induce their distortion and formation of pores that can provide a pathway for the penetration of the succeeding Pc molecules and thus explains increased phototoxicity of ZnPc-6SQ at high concentrations. Much bigger size of PSs seems to be an obstacle for intramolecular accumulation.²⁹ Nevertheless, large fullerene-based PSs can achieve up to 6 logs of killing at 10 μ M concentration and 2 J/cm 2 white light.³⁰ However, one should consider that though in organic solvents or hydrophobic environments, fullerenes are very efficient in producing photoexcited $^1\text{O}_2$, in aqueous environments, they switch the photochemical mechanism to Type 1 producing hydroxyl radicals, which is known to be the most biologically active free radical and can be formed also under hypoxic conditions.

Conclusions

In conclusion, three Zn(II)Pc derivatives were synthesized, characterized and their antimicrobial photodynamic efficacy against monospecies of Gram-negative *E. coli* cells was assessed. The rational design involved the substitution of the Zn(II)Pc ring with thiophenyl groups that confers favorable characteristics to PS, such as red shift of absorption maxima, increased singlet oxygen quantum yield, lowered aggregation. However, photobiological studies indicate that overall activity depends on the flexibility of the molecule. To the best of our knowledge, this is the first clear example showing the impact of the morphology of the phthalocyanine-based PS on its photodynamic efficacy against Gram-negative bacteria. Though for the systematic study a library of compounds should be prepared and assayed for their activity, this elegant comparison shows that membrane accumulation is significant for PSs that carry out largely Type 2 photochemistry. Indeed, for phthalocyanine-based PS DNA photocleavage could only be observed after a long period of irradiation, when the bacterial cells are largely photoinactivated.³¹ Comparison of the activity of these exemplary PSs indicates that tightly packed phospholipids of the outer membrane of Gram-negative bacteria do not leave much space for rapid internalization of bulky PSs. Molecular level control of the morphology of PSs will help to achieve efficient aPDT treatment with short exposure time, low PS concentration, and mild irradiation.

Experimental

Synthesis and Characterization

Synthetic procedures were carried out under dry argon atmosphere, unless otherwise specified. All reagents and solvents were purchased at the highest commercial quality available and used without further purification. Column chromatography was carried out on silica gel Merck-60 (230–400 mesh, 60 Å), and TLC on polyester sheets pre-coated with silica gel 60 F254 (Macherey-Nagel). NMR spectra were recorded on an ARX 300 or an AMX 400 from Bruker

Analytische Messtechnik (Karlsruhe, Germany) spectrometer at a constant temperature of 298 K. Chemical shifts δ are given relative to TMS ($d = 0$) and referenced to the solvent signal. Electrospray ionization (ESI) mass spectra were recorded on a Bruker Daltonics (Bremen, Germany) MicroTof with loop injection. MALDI-TOF MS were recorded with a Bruker Reflex III spectrometer.

Synthesis of ZnPc-0S: A mixture of phthalonitrile **1** (250 mg, 0.64 mmol) and the unsubstituted phthalonitrile **2** (328 mg, 2.56 mmol) in *n*-pentanol (30 mL) was heated to 120°C. A piece of lithium chip (44.8 mg, 6.4 mmol) was then added. The mixture was stirred at 120–130°C for 12 h under argon atmosphere, and then Zn(OAc)₂·2H₂O (700 mg, 3.2 mmol) was added. The mixture was kept stirring at this temperature for a further 5 h. After cooling, the mixture as evaporated under reduced pressure and purified by silica gel column chromatography using CHCl₃/CH₃OH/Et₃N (200:40:1, v/v/v) as the eluent, followed by recrystallization from tetrahydrofuran to give a blue solid (74 mg, 14%). ¹H NMR (CDCl₃ with a trace amount of pyridine-*d*5): 9.30 (d, 1H), 8.98–9.08 (m, 4H), 8.85–8.88 (m, 2H), 7.92–8.31 (m, 3H), 7.75–7.90 (m, 6H), 7.62 (s, 1H), 3.27–3.35 (m, 6H), 2.34 (d, 12H), 1.87 (s, 6H). MALDI-MS *m/z*: calcd for C₄₇H₄₁N₁₁OZnH 840.2865, found 840.11.

Synthesis of ZnPc-3S: A mixture of phthalonitrile **1** (391 mg, 1 mmol) and the 3-phenylthio phthalonitrile **3** (944 mg, 4 mmol) in *n*-pentanol (35 mL) was heated to 120°C. A piece of lithium chip (70 mg, 10 mmol) was then added. The mixture was stirred at 120–130°C for 5 h, and then Zn(OAc)₂·2H₂O (1.1 g, 5 mmol) was added. The mixture was kept stirring at this temperature for a further 5 h. After cooling, the mixture as evaporated under reduced pressure and purified by silica gel column chromatography using CHCl₃/CH₃OH/Et₃N (200:40:1, v/v/v) as the eluent, to give a green solid (128 mg, 11%). ¹H NMR (CDCl₃ with a trace amount of pyridine-*d*5) 9.01–9.31 (m, 4H), 7.72–8.04 (m, 9H), 7.29–7.60 (m, 16H), 3.49–3.78 (m, 6H), 2.21–2.35 (m, 12H), 1.89–1.99 (m, 6H). MALDI-MS *m/z*: calcd for C₆₅H₅₃N₁₁OS₃Zn 1163.2888, calcd for C₆₅H₅₃N₁₁OS₃ZnH 1164.2966.

Synthesis of ZnPc-6S: A mixture of phthalonitrile **1** (391 mg, 1 mmol) and the 3,6-bis(phenylthio)phthalonitrile **4** (1376 mg, 4 mmol) in *n*-pentanol (35 mL) was heated to 120°C. A piece of lithium chip (70 mg, 10 mmol) was then added. The mixture was stirred at 120–130°C for 5 h, the solvent removed and purified by silica gel column chromatography using CHCl₃/CH₃OH (10:1, v/v) as the eluent. Compound **5** was dissolved in DMF and Zn(OAc)₂·2H₂O (1.1 g, 5 mmol) was added. The mixture was stirred at 120°C for a further 5 h. After cooling, the mixture as evaporated under reduced pressure and purified by silica gel column chromatography using CHCl₃/CH₃OH (10:1, v/v) as the eluent (104 mg, 7%). ¹H NMR (DMSO-*d*6 with a trace amount of pyridine-*d*5) 6.60–9.81 (m, 41H), 4.06–4.72 (m, 6H), 2.00–2.76 (m, 18H). MALDI-MS *m/z*: calcd for C₈₃H₆₅N₁₁OS₆Zn 1487.30, found 1487.15.

Synthesis of ZnPc-0SQ: A mixture of ZnPc-0S (84 mg, 0.10 mmol) and iodomethane (1.42 g, 0.01 mol) in DMF (8 mL) was stirred at 50°C temperature for 14h in the absence of light. The volatiles was removed under reduced pressure. Diethyl ether (25 mL) was added to wash the residue, which was then dissolved in DMSO (3 mL) and re-precipitated by the addition of diethyl ether. After centrifugation, the blue solid was washed with CH₂Cl₂ (3x10 mL) and then dried in vacuo (75 mg, 82%). ¹H NMR (DMSO-*d*6 with a trace amount of pyridine-*d*5): 9.51 (d, 1H), 9.05–9.38 (m, 6H), 8.96 (d, 1H), 8.07–8.36 (m, 8H), 7.11 (d, 1H), 5.02 (s, 2H), 4.71–4.89 (dd, 4H), 3.45–3.50 (m, 27H). ¹H, ¹H GCOSY (500 MHz / 500 MHz, DMSO-*d*6 with a trace amount of pyridine-*d*5 [selected traces]: $\delta^1\text{H} / \delta^1\text{H}$: 9.54/8.34; 9.40/8.21; 9.33/8.16; 9.23/8.13; 9.09/8.08; 8.99/8.26; 8.21/7.10. HRMS *m/z*: calcd for C₅₀H₅₀N₁₁OIZn [M]²⁺ 505.62625, found 505.62647; calcd for C₅₀H₅₀N₁₁OI₂Zn [M]⁺ 1138.15751, found 1138.15928.

Synthesis of ZnPc-3SQ: A mixture of ZnPc-3S (116 mg, 0.10 mmol) and iodomethane (1.42 g, 0.01 mol) in DMF (8 mL) was stirred at 50°C for 14 h in the absence of light. The volatiles were removed under reduced pressure. The green solid was washed with MeOH (3x10 mL) and then dried in vacuo (109 mg, 68%). ¹H NMR (500 MHz, DMSO-*d*6 with a trace amount of pyridine-*d*5): 9.03–9.32 (m, 3H), 7.97–8.79 (m, 8H), 6.57–7.83 (m, 13H), 4.58–5.18 (m, 6H), 2.98–3.50 (m, 27H). ¹H, ¹H GCOSY (500 MHz / 500 MHz, DMSO-*d*6 with a trace amount of pyridine-*d*5 [selected traces]: $\delta^1\text{H} / \delta^1\text{H}$: 9.28/4.69; 8.13/4.75; 9.31/8.17; 9.26/8.05; 8.63/7.95; 8.77/8.41; 8.61/7.99; 8.63/7.95; 8.16/7.56; 8.12/7.26; 8.03/7.24; 7.96/7.38; 7.89/7.23; 8.13/7.06; 7.62/6.59; 7.38/6.45; 5.12/4.79; 4.56/4.11; 4.50/4.22; 4.45/3.97; 5.13/3.07; 4.75/3.20; 4.55/3.18; 4.24/3.17. HRMS *m/z*: calcd for C₆₈H₆₂N₁₁OS₃I₂Zn [M]²⁺ 667.63131, found 667.63169; calcd for C₆₈H₆₂N₁₁OS₃I₂Zn [M]⁺ 1462.16763, found 1462.16896.

Synthesis of ZnPc-6SQ: A mixture of ZnPc-6S (149 mg, 0.10 mmol) and iodomethane (1.42 g, 0.01 mol) in DMF (8 mL) was stirred at 50°C for 14h in the absence of light. The volatiles were removed under reduced pressure. The green solid was washed with MeOH (3x10 mL) and then dried in vacuo (ca. 150 mg, 78%). ¹H NMR (DMSO-*d*6 with a trace amount of pyridine-*d*5): 9.32–9.36 (m, 1H), 7.02–8.55 (m, 40H), 5.07 (d, 2H), 4.71 (d, 4H), 2.86–3.23 (m, 27H). ¹H, ¹H GCOSY (500 MHz / 500 MHz, DMSO-*d*6 with a trace amount of pyridine-*d*5 [selected traces]: $\delta^1\text{H} / \delta^1\text{H}$: 9.36/8.18; 8.47/7.42; 7.95/7.16; 7.79/6.80; 7.46/7.09; 7.62/6.56; 8.18/4.73; 5.09/4.69; 4.73/3.14. HRMS *m/z*: calcd for C₈₆H₇₄N₁₁OS₆I₂Zn [M]²⁺ 830.63642, found 830.63803; calcd for C₈₆H₇₄N₁₁OS₆I₂Zn [M]⁺ 1788.17786, found 1788.17551

Photophysical characterization

Absorption spectra were measured on Agilent 8453 spectrophotometer and baseline corrected. Steady-state emission spectra were recorded on a HORIBA Jobin-Yvon IBH FL-322 Fluorolog 3 spectrometer equipped with a 450 W xenon-arc lamp, double-grating excitation and emission

monochromators (2.1 nm/mm dispersion; 1200 grooves/mm). All solvents used were of the spectrometric grade. All experiments were performed at room temperature.

Fluorescence quantum yields

Fluorescence quantum yields (Φ_F) were determined by a comparative method using the following equation:

$$\Phi = \Phi_s \cdot (n/n_s) \cdot (F/F_s) \cdot (1 - 10^{-A_s}) / (1 - 10^{-A})$$

Where F are areas under fluorescence emission curves of the samples and F_s of ZnPc as standard. A and A_s are the absorbances of the samples and standard at the excitation wavelength and n and n_s are refractive indices of solvents used for samples and standard, respectively. ZnPc in DMF was used as a standard, $\Phi_F=0.28$. The absorbance of the solutions at the excitation wavelength ranged between 0.05 and 0.1.

Singlet oxygen quantum yields

Singlet oxygen quantum yields were determined using the relative method. Polychromatic irradiation from a projector lamp passing through a cut-off filter at 610 nm was used to carry out the experiments. Freshly prepared dye solution in dark flasks were mixed with the PSs only immediately before taking the samples at "0 time." $^1\text{O}_2$ photogeneration rates in DMF were derived using 1,3-diphenylisobenzofuran (DPBF). The initial absorbance of DPBF was adjusted to about 1.0, then the PS was added to reach absorbance about 0.2-0.3. The photooxidation of DPBF was monitored between 0 s to 25 s. $^1\text{O}_2$ photogeneration rates in water were derived using 9,10-anthracenediyl-bis(methylene)dimalonic acid (ABMDMA) as a fluorescent monitor ($\lambda_{\text{exc}} = 370$ nm) for photosensitized bleaching rates monitored between 0 s to 80 s. The Φ_Δ for the samples was calculated according to the following equation:

$$\Phi_\Delta^S = \Phi_\Delta^R \cdot \frac{r_S}{r_R} \cdot \frac{\int_{\lambda_1}^{\lambda_2} I(\lambda) \cdot (1 - 10^{-A_R(\lambda)}) \cdot d\lambda}{\int_{\lambda_1}^{\lambda_2} I(\lambda) \cdot (1 - 10^{-A_S(\lambda)}) \cdot d\lambda}$$

where r is the slope of the monitor's bleaching over time (plotted as $\ln(A_0/A)$ for DPBF and as emission intensity integral for ABMDMA), $\lambda_1 - \lambda_2$ is the irradiation wavelength interval, $I_0(\lambda)$ the incident spectral photon flow, $A(\lambda)$ the absorbance, and the subscripts R and S are the reference (zinc phthalocyanine $\Phi_\Delta = 0.56$ in DMF and methylene blue, $\Phi_\Delta = 0.52$ in H_2O) and sample, respectively. The incident intensity can be approximated by a constant value, drawn out of the integral and canceled.

Partition coefficients

1-Octanol/water partition coefficients ($\log P_{o/w}$) were determined at 25°C using equal volumes of water (1 mL) and 1-octanol (1 mL). The final concentration of compound was approx. 25 μM . The mixture was stirred for 1h and centrifuged (10 min, 4400 rpm) to enable a phase separation. An aliquot (50 μL) of aqueous and organic phases were dissolved in 1 mL

of N,N -dimethylformamide (DMF) and final concentration determined by absorption spectroscopy. $\log P_{o/w}$ was calculated according to the following equation:

$$\log P_{o/w} = \log ([\text{PS}]_{\text{octanol}} / [\text{PS}]_{\text{water}})$$

DFT calculations

Geometries were optimized by means of density functional theory (DFT) method. B3LYP was used in the Gaussian 09 program.³² For all calculations, we used the 6-311G (d, p) basis set for all atoms. No imaginary frequency was obtained ($\text{NImag} = 0$). Simulated electronic spectra were computed on the optimized geometry at S_0 by means of time-dependent density functional theory (TD-DFT) calculations. All the calculations were performed for vacuum conditions.

Bacterial culture

Escherichia coli strains 536 (O6:K15:H31) and UTI89 are an archetypal uropathogenic *E. coli* isolates from a case of pyelonephritis. The *E. coli* strains were maintained on Luria-Bertani (LB) broth agar and were stored at 4°C. A single isolated colony was picked from this plate, transferred in 3 mL LB broth and incubated aerobically at 37 °C overnight in a rotary incubator with shaking at 180 rpm (rotations per minute). On the next day the bacteria were suspended in 20 mL of fresh LB medium to an optical density (OD_{600}) of 0.1 and grown in a flask to an attenuation of ca. $\text{OD}_{600}=0.4$. The bacterial suspension was then centrifuged at 4000 rpm for 5 min, resuspended in PBS to the final bacterial concentration of ca. 1×10^9 cells per mL and subsequently used for the experiments.

Photoinactivation of bacterial cells in planktonic cultures

To induce $^1\text{O}_2$ generation the 1 mL PS stained bacteria (15 min, 37 °C) were placed in 24-well plate and were irradiated with LED light source having emission maximum at 660nm or 730nm from the top of the plate. Fluence rates were routinely measured using power meter (Solar Meter from Solartech). After irradiation, the living bacterial cells were determined by serial dilutions of the bacterial suspension and plating on LB agar plates. The plates were incubated overnight at 37 °C and the number of CFU/mL was determined. As controls, PS treated bacteria were kept in the dark (dark control) and untreated bacteria were exposed to light (light control).

Conflicts of interest

There are no conflicts to declare.

Acknowledgments

This research has been supported by the Deutsche Forschungsgemeinschaft (DFG) project GA 2362/1-1 to AG and SFB 1009, TP B05 to UD. AG acknowledges support from the

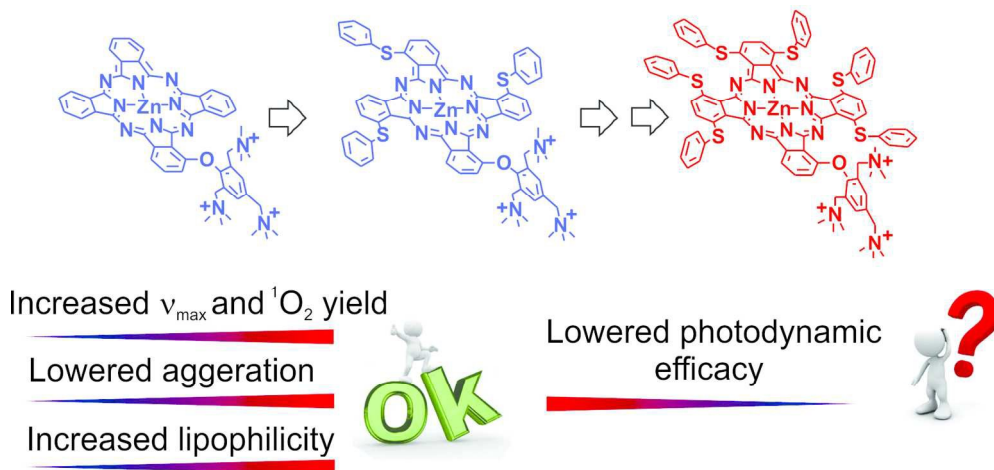
ARTICLE

Journal Name

Fonds der Chemischen Industrie, WWU Graduate Center and Santander Universities.

Notes and references

- (a) M. Wainwright, T. Maisch, S. Nonell, K. Plaetzer, A. Almeida, G. P. Tegos and M. R. Hamblin, *Lancet Infect. Dis.*, 2016, **3099**, 1–7, (b) F. Cieplik, L. Tabenski, W. Buchalla and T. Maisch, *Front. Microbiol.*, 2014, **5**, 405.
- (a) M. R. Hamblin, *Curr. Opin. Microbiol.*, 2016, **33**, 67–73; (b) M. Wainwright, *J. Antimicrob. Chemother.*, 2012, **67**, 787–788.
- Y. Liu, R. Qin, S. A. J. Zaat, E. Breukink and M. Heger, *J. Clin. Transl. Res.*, 2015, **1**, 140–167.
- M. Wainwright and A. McLean, *Dye. Pigment.*, 2017, **136**, 590–600.
- (a) J. M. Dąbrowski, B. Pucelik, A. Regiel-Futyra, M. Brindell, O. Mazuryk, A. Kyzioł, G. Stochel, W. Macyk and L. G. Arnaut, *Coord. Chem. Rev.*, 2016, **325**, 67–101; (b) M. Tim, *J. Photochem. Photobiol. B Biol.*, 2015, **150**, 2–10.
- E. Alves, M. A. Faustino, M. G. Neves, A. Cunha, J. Tome and A. Almeida, *Future Med. Chem.*, 2014, **6**, 141–64.
- M. R. Ke, J. M. Eastel, K. L. K. Ngai, Y. Y. Cheung, P. K. S. Chan, M. Hui, D. K. P. Ng and P. C. Lo, *Recent Pat Antiinfect Drug Discov*, 2013, **8**, 1–23.
- A. Galstyan, R. Schiller and U. Dobrindt, *Angew. Chemie Int. Ed.*, 2017, **56**, 10498–10502; A. Galstyan, R. Schiller and U. Dobrindt, *Angew. Chemie*, 2017, **129**, 10498–10502
- M. R. Ke, J. M. Eastel, K. L. K. Ngai, Y. Y. Cheung, P. K. S. Chan, M. Hui, D. K. P. Ng and P. C. Lo, *Eur. J. Med. Chem.*, 2014, **84**, 278–283.
- X. Ragàs, X. He, M. Agut, M. Roxo-Rosa, A. R. Gonsalves, A. C. Serra and S. Nonell, *Molecules*, 2013, **18**, 2712–25.
- S. P. Denyer, J. Y. Maillard, *J. Appl. Microbiol.*, 2002, **92**, 35–45.
- A. Galstyan, D. Block, S. Niemann, M. C. Grüner, S. Abbruzzetti, M. Oneto, C. G. Daniliuc, S. Hermann, C. Viappiani, M. Schäfers, B. Löffler, C. A. Strassert and A. Faust, *Chem. - A Eur. J.*, 2016, **22**, 5243–5252.
- R. M. Cordeiro, R. Miotto and M. S. Baptista, *J. Phys. Chem. B*, 2012, **116**, 14618–14627.
- A. Galstyan, J. Putze and U. Dobrindt, *Chem. - A Eur. J.*, 2018, **24**, 1178–1186.
- K. Alenezi, A. Tovmasyan, I. Batinic-Haberle and L. T. Benov, *Photodiagnosis Photodyn. Ther.*, 2017, **17**, 154–159.
- V. N. Mantareva, I. Angelov, D. Wöhrle, E. Borisova and V. Kussovski, *J. Porphyr. Phthalocyanines*, 2013, **17**, 399–416.
- D. Vecchio, B. Bhayana, L. Huang, E. Carrasco, C. L. Evans and M. R. Hamblin, *Eur. J. Med. Chem.*, 2014, **75**, 479–491.
- (a) L. B. Josefsen and R. W. Boyle, *Theranostics*, 2012, **2**, 916–966; (b) Bonnett, *Chem. Soc. Rev.*, 1995, **24**, 19–33; (c) F. Dumoulin, M. Durmuş, V. Ahsen and T. Nyokong, *Coord. Chem. Rev.*, 2010, **254**, 2792–2847.
- (a) T. Furuyama, K. Satoh, T. Kushiya and N. Kobayashi, *J. Am. Chem. Soc.*, 2014, **136**, 765–776; (b) N. Kobayashi, T. Furuyama and K. Satoh, *J. Am. Chem. Soc.*, 2011, **133**, 19642–19645; (c) N. Kobayashi, H. Ogata, N. Nonaka and E. a. Luk'yanets, *Chem. - A Eur. J.*, 2003, **9**, 5123–5134.
- (a) A. Galstyan, K. Riehemann, M. Schäfers, A. Faust and A. Faust, *J. Mater. Chem. B*, 2016, **4**, 5683–5691; (b) M. M. Ayhan, G. Altınbaş Özpınar, M. Durmuş and A. G. Gürek, *Dalt. Trans.*, 2013, **42**, 14892–904.
- X. S. Li, J. Guo, J. J. Zhuang, B. Y. Zheng, M. R. Ke and J. D. Huang, *Bioorganic Med. Chem. Lett.*, 2015, **25**, 2386–2389.
- P. Tau and T. Nyokong, *Dalt. Trans.*, 2006, 4482.
- M. Machacek, A. Cidlina, V. Novakova, J. Svec, E. Rudolf, M. Miletin, R. Kučera, T. Simunek and P. Zimcik, *J. Med. Chem.*, 2015, **58**, 1736–1749.
- (a) Y. Zorlu, U. Kumru, Ü. İşci, B. Divrik, E. Jeanneau, F. Albrieux, Y. Dede, V. Ahsen and F. Dumoulin, *Chem. Commun.*, 2015, **51**, 6580–6583; (b) N. Kobayashi, T. Fukuda, K. Ueno and H. Ogino, *J. Am. Chem. Soc.*, 2001, **123**, 10740; (c) Y. Gao, Y. Chen, R. Li, Y. Bian, X. Li and J. Jiang, *Chem. - Eur. J.*, 2009, **15**, 13241.
- I. Scalise and E. N. Durantini, *Bioorg. Med. Chem.*, 2005, **13**, 3037–3045.
- F. Giuliani, M. Martinelli, A. Cocchi, D. Arbia, L. Fantetti and G. Roncucci, *Antimicrob. Agents Chemother.*, 2010, **54**, 637–642.
- M. R. Ke, J. M. Eastel, K. L. K. Ngai, Y. Y. Cheung, P. K. S. Chan, M. Hui, D. K. P. Ng and P. C. Lo, *Chem. - An Asian J.*, 2014, **9**, 1868–1875.
- P. S. Orekhov, E. G. Kholina, M. E. Bozdoganyan, A. M. Nesterenko, I. B. Kovalenko and M. G. Strakhovskaya, *J. Phys. Chem. B*, 2018, **122**, 3711–3722.
- P.-C. Hsu, D. Jefferies and S. Khalid, *J. Phys. Chem. B*, 2016, **120**, 11170–11179.
- G. P. Tegos, T. N. Demidova, D. Arcila-Lopez, H. Lee, T. Wharton, H. Gali and M. R. Hamblin, *Chem. Biol.*, 2005, **12**, 1127–1135.
- M. B. Spesia, D. A. Caminos, P. Pons and E. N. Durantini, *Photodiagnosis Photodyn. Ther.*, 2009, **6**, 52–61.
- M. J. Frisch, G. W. Trucks, H. B. Schlegel, G. E. Scuseria, M. A. Robb, J. R. Cheeseman, G. Scalmani, V. Barone, B. Mennucci, G. A. Petersson, H. Nakatsuji, M. Caricato, X. Li, H. P. Hratchian, A. F. Izmaylov, J. Bloino, G. Zheng, J. L. Sonnenberg, M. Hada, M. Ehara, K. Toyota, R. Fukuda, J. Hasegawa, M. Ishida, T. Nakajima, Y. Honda, O. Kitao, H. Nakai, T. Vreven, J. A. Montgomery Jr., J. E. Peralta, F. Ogliaro, M. Bearpark, J. J. Heyd, E. Brothers, K. N. Kudin, V. N. Staroverov, R. Kobayashi, J. Normand, K. Raghavachari, A. Rendell, J. C. Burant, S. S. Iyengar, J. Tomasi, M. Cossi, N. Rega, J. M. Millam, M. Klene, J. E. Knox, J. B. Cross, V. Bakken, C. Adamo, J. Jaramillo, R. Gomperts, R. E. Stratmann, O. Yazyev, A. J. Austin, R. Cammi, C. Pomelli, J. W. Ochterski, R. L. Martin, K. Morokuma, V. G. Zakrzewski, G. A. Voth, P. Salvador, J. J. Dannenberg, S. Dapprich, A. D. Daniels, Ö. Farkas, J. B. Foresman, J. V. Ortiz, J. Cioslowski and D. J. Fox, *Gaussian, Inc. Wallingford CT*, 2009, 2–3.



152x72mm (300 x 300 DPI)